

000  
001  
002  
003  
004 **Supplementary Material to “External Prior Guided Internal Prior Learning for**  
005 **Real Noisy Image Denoising”**  
006  
007  
008  
009                   Anonymous CVPR submission  
010  
011                   Paper ID 1047  
012  
013  
014  
015  
016  
017  
018  
019  
020  
021  
022  
023  
024  
025  
026  
027  
028  
029  
030  
031  
032  
033  
034  
035  
036  
037  
038  
039  
040  
041  
042  
043  
044  
045  
046  
047  
048  
049  
050  
051  
052  
053  
054  
055  
056  
057  
058  
059  
060  
061  
062  
063  
064  
065

In this supplementary material, we provide:

1. The closed-form solution of the sparse coding problem (6) in the main paper.
  2. More denoising results on the real noisy images in dataset [1].
  3. More results on the 15 cropped real noisy images (with mean image of 500 shots as “ground truth”) in dataset [2].
  4. More results on the 60 cropped real noisy images (with mean image of 500 shots as “ground truth”) in dataset [2].

## 1. Closed-Form Solution of the Weighted Sparse Coding Problem (6)

For notation simplicity, we ignore the indices  $n, m, t$  in problem (6) of the main paper. It turns into the following weighted sparse coding problem:

$$\min_{\boldsymbol{\alpha}} \|\mathbf{y} - \mathbf{D}\boldsymbol{\alpha}\|_2^2 + \sum_{j=1}^{sp} \lambda_j |\alpha_j|. \quad (1)$$

Since  $D$  is an orthogonal matrix, problem (1) is equivalent to:

$$\min_{\boldsymbol{\alpha}} \|\mathbf{D}^T \mathbf{y} - \boldsymbol{\alpha}\|_2^2 + \sum_{j=1}^{3p^2} \lambda_j |\alpha_j|. \quad (2)$$

For simplicity, we denote  $\mathbf{z} = \mathbf{D}^T \mathbf{y}$ . Here we have  $\lambda_j > 0$ ,  $j = 1, \dots, 3p^2$ , then problem (2) can be written as:

$$\min_{\boldsymbol{\alpha}} \sum_{j=1}^{3p^2} ((\mathbf{z}_j - \boldsymbol{\alpha}_j)^2 + \lambda_j |\boldsymbol{\alpha}_j|). \quad (3)$$

The problem (3) is separable w.r.t. each  $\alpha_i$ , and hence can be simplified to  $3p^2$  independent scalar minimization problems:

$$\min_{\boldsymbol{\alpha}_j} (\mathbf{z}_j - \boldsymbol{\alpha}_j)^2 + \lambda_j |\boldsymbol{\alpha}_j|, \quad (4)$$

where  $j = 1, \dots, 3p^2$ . Taking derivative of  $\alpha_j$  in problem (4) and setting the derivative to be zero. There are two cases for the solution.

(a) If  $\alpha_j > 0$ , we have

$$2(\alpha_j - \mathbf{z}_j) + \lambda_j = 0. \quad (5)$$

The solution is

$$\hat{\alpha}_j = \mathbf{z}_j - \frac{\lambda_j}{2} \geq 0. \quad (6)$$

So  $\mathbf{z}_j \geq \frac{\lambda_j}{2} > 0$ , and the solution  $\hat{\alpha}_j$  can be written as:

$$\hat{\alpha}_j = \text{sgn}(\mathbf{z}_j) * (|\mathbf{z}_j| - \frac{\lambda_j}{2}), \quad (7)$$

where  $\text{sgn}(\bullet)$  is the sign function.

(b) If  $\alpha_j < 0$ , we have

$$2(\alpha_j - \mathbf{z}_j) - \lambda_j = 0. \quad (8)$$

The solution is

$$\hat{\alpha}_j = \mathbf{z}_j + \frac{\lambda_j}{2} < 0. \quad (9)$$

108 So  $\mathbf{z}_j < -\frac{\lambda_j}{2} < 0$ , and the solution  $\hat{\alpha}_j$  can be written as:  
 109

$$\hat{\alpha}_j = \text{sgn}(\mathbf{z}_j) * (-\mathbf{z}_j - \frac{\lambda_j}{2}) = \text{sgn}(\mathbf{z}_j) * (|\mathbf{z}_j| - \frac{\lambda_j}{2}). \quad (10)$$

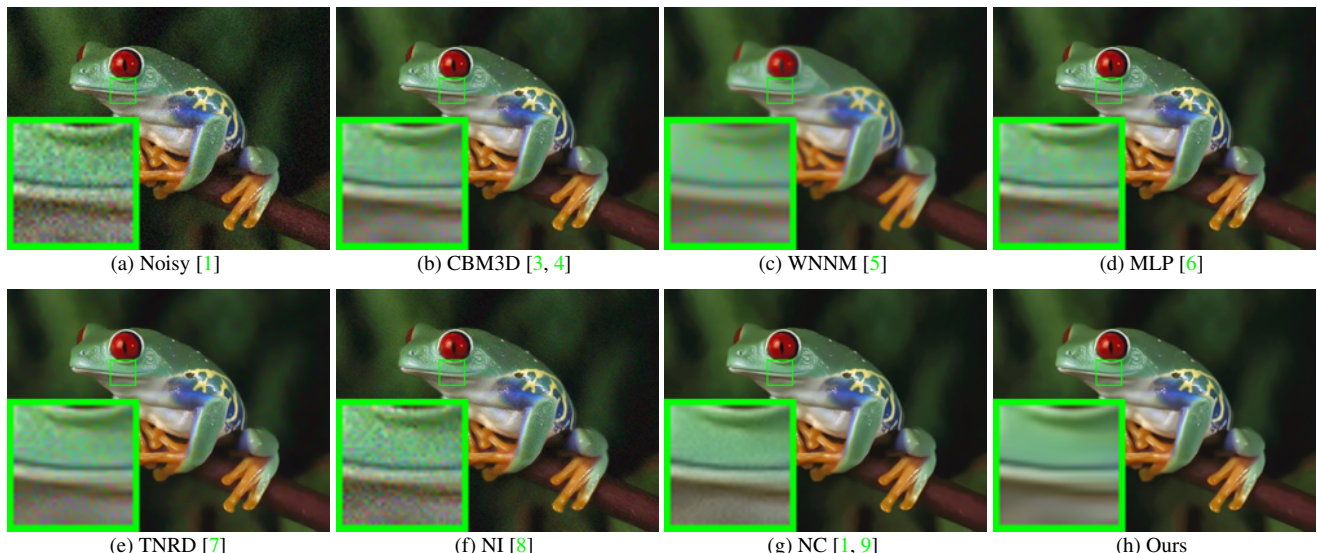
110 In summary, we have the final solution of the weighted sparse coding problem (1) as:  
 111

$$\hat{\alpha} = \text{sgn}(\mathbf{D}^T \mathbf{y}) \odot \max(|\mathbf{D}^T \mathbf{y}| - \lambda, 0), \quad (11)$$

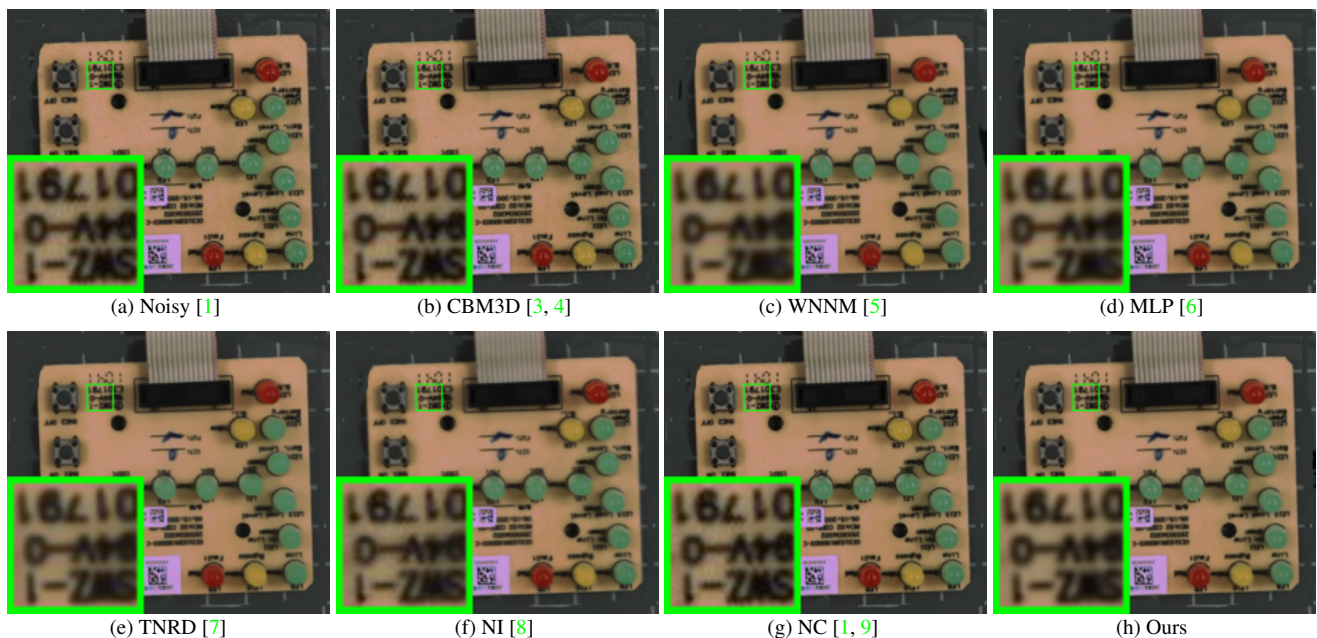
112 where  $\lambda = \frac{1}{2}[\lambda_1, \lambda_2, \dots, \lambda_{3p^2}]^\top$  is the vector of regularization parameter and  $\odot$  means element-wise multiplication.  
 113

## 114 2. More Denoising Results on the Real Noisy Images in Dataset [1]

115 In this section, we give more comparisons of the competing methods on the dataset [1]. The real noisy images in dataset  
 116 [1] have no “ground truth” images and hence we only compare the visual quality of the denoised images by different methods.  
 117 As can be seen from Figures 1-4, our proposed method performs better than the state-of-the-art denoising methods.  
 118



119 Figure 1. Denoised images of the real noisy image “Frog” [1] by different methods. The images are better to be zoomed in on screen.  
 120



121 Figure 2. Denoised images of the real noisy image “Circuit” [1] by different methods. The images are better to be zoomed in on screen.  
 122

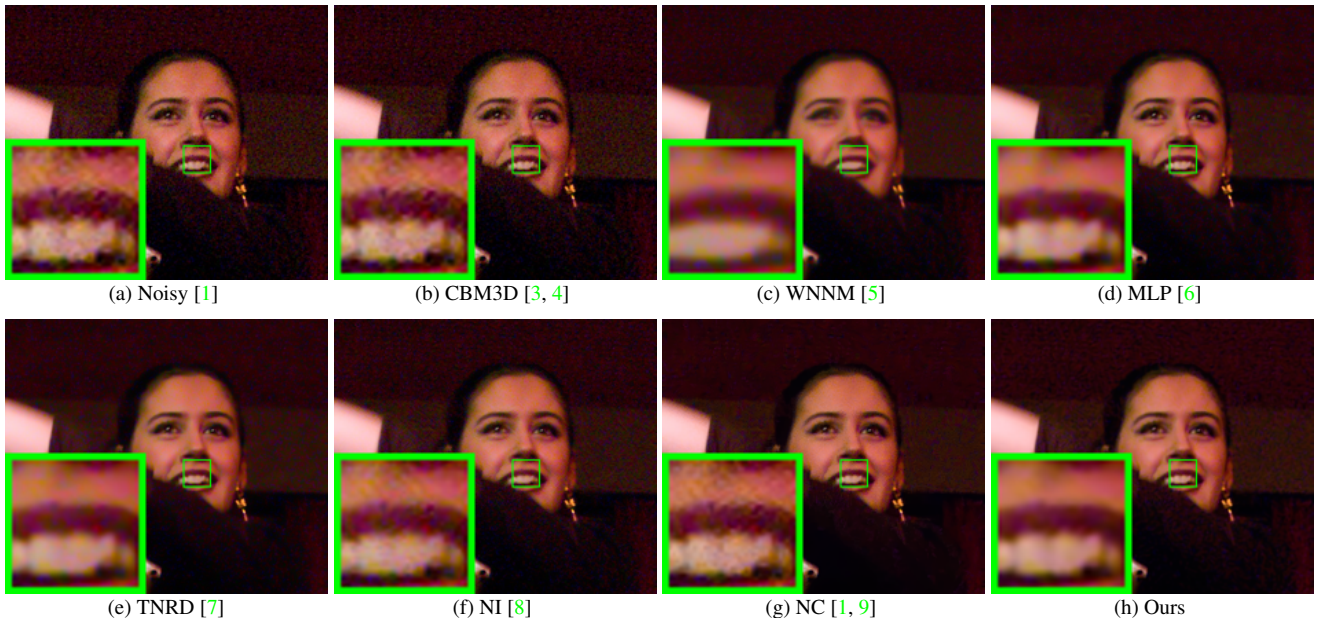
216  
217  
218  
219  
220  
221  
222  
223  
224  
225  
226

Figure 3. Denoised images of the real noisy image “Woman” [1] by different methods. The images are better to be zoomed in on screen.

236

237

238

239

240

241

242

243

244

245

246

247

248

249

250

251

252

253

254

255

256

257

258

259

260

261

262

263

264

265

266

267

268

269

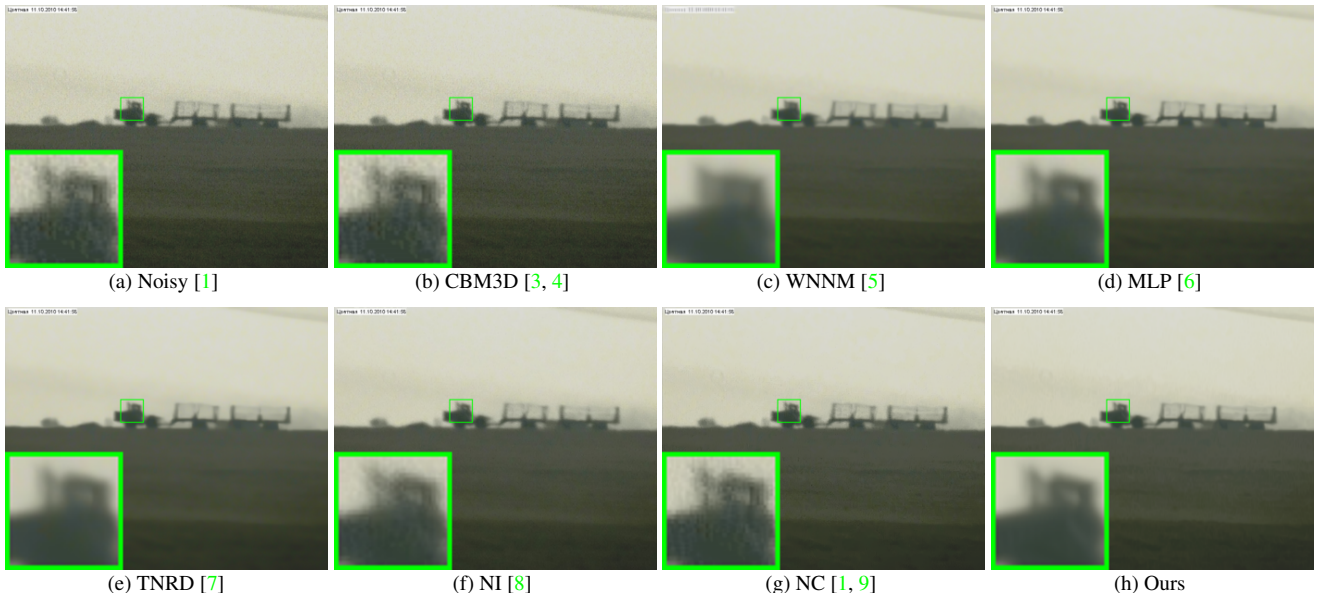
270  
271  
272  
273  
274  
275  
276  
277  
278  
279  
280  
281  
282  
283  
284  
285  
286  
287  
288  
289  
290  
291  
292  
293  
294  
295  
296  
297  
298  
299  
300  
301  
302  
303  
304  
305  
306  
307  
308  
309  
310  
311  
312  
313  
314  
315  
316  
317  
318  
319  
320  
321  
322  
323

Figure 4. Denoised images of the real noisy image “Vehicle” [1] by different methods. The images are better to be zoomed in on screen.

### 3. More Denoising Results on the 15 Cropped Images Used in [2]

In this section, we provide more visual comparisons of the proposed method with the state-of-the-art denoising methods on the 15 cropped real noisy images used in [2]. In this dataset, each scene was shot 500 times under the same camera and camera setting. The mean image of the 500 shots is roughly taken as the “ground truth”, with which the PSNR can be computed. As can be seen from Figures 5-9, in most cases, our proposed method achieves better performance than the competing methods. This validates the effectiveness of our proposed external prior guided internal prior learning framework for real noisy image denoising.

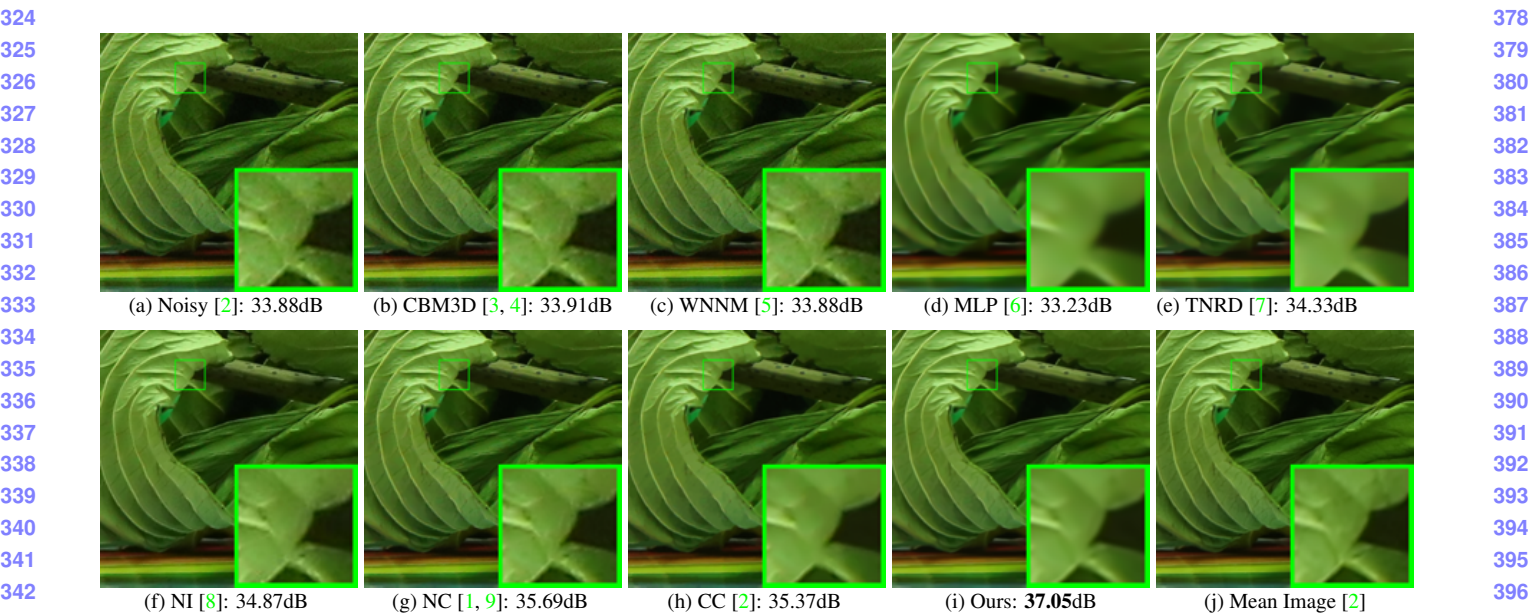


Figure 5. Denoised images of a region cropped from the real noisy image “Canon 5D Mark 3 ISO 3200 2” [2] by different methods. The images are better to be zoomed in on screen.

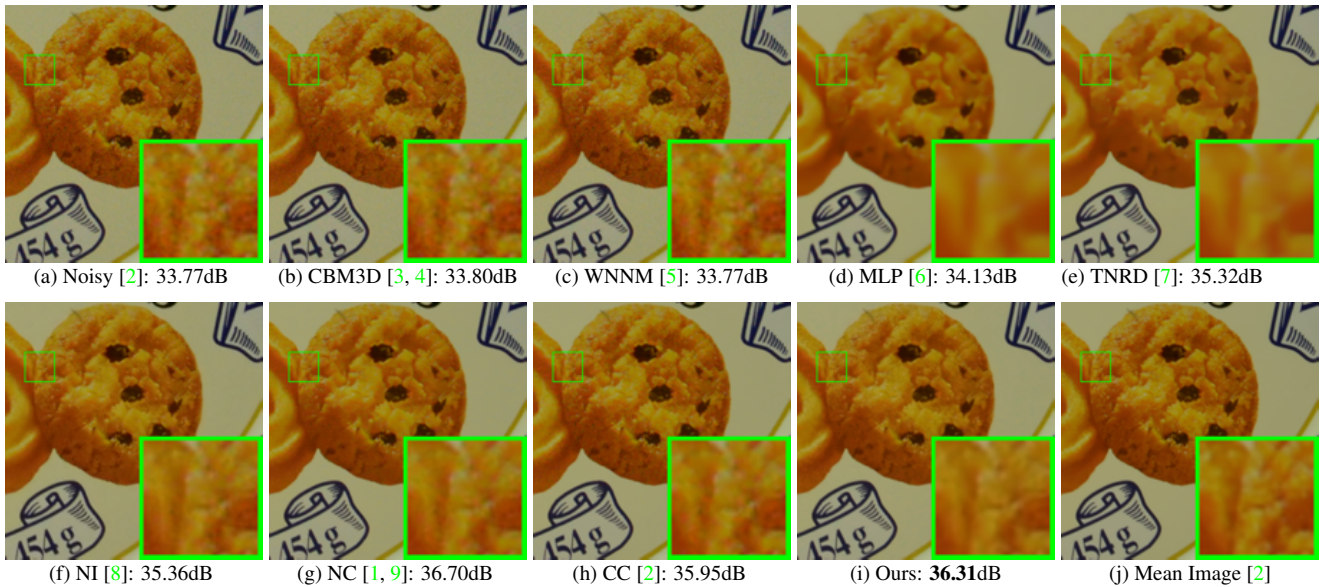


Figure 6. Denoised images of a region cropped from the real noisy image “Nikon D600 ISO 3200 2” [2] by different methods. The images are better to be zoomed in on screen.

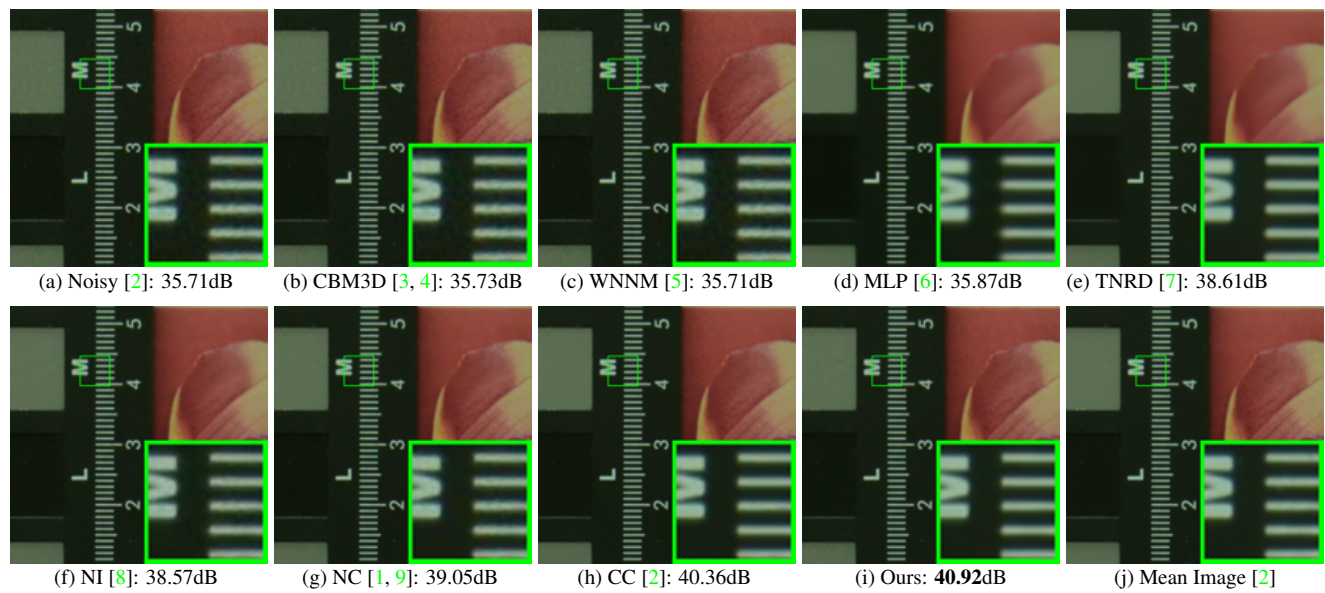


Figure 7. Denoised images of a region cropped from the real noisy image “Nikon D800 ISO 1600 2” [2] by different methods. The images are better to be zoomed in on screen.

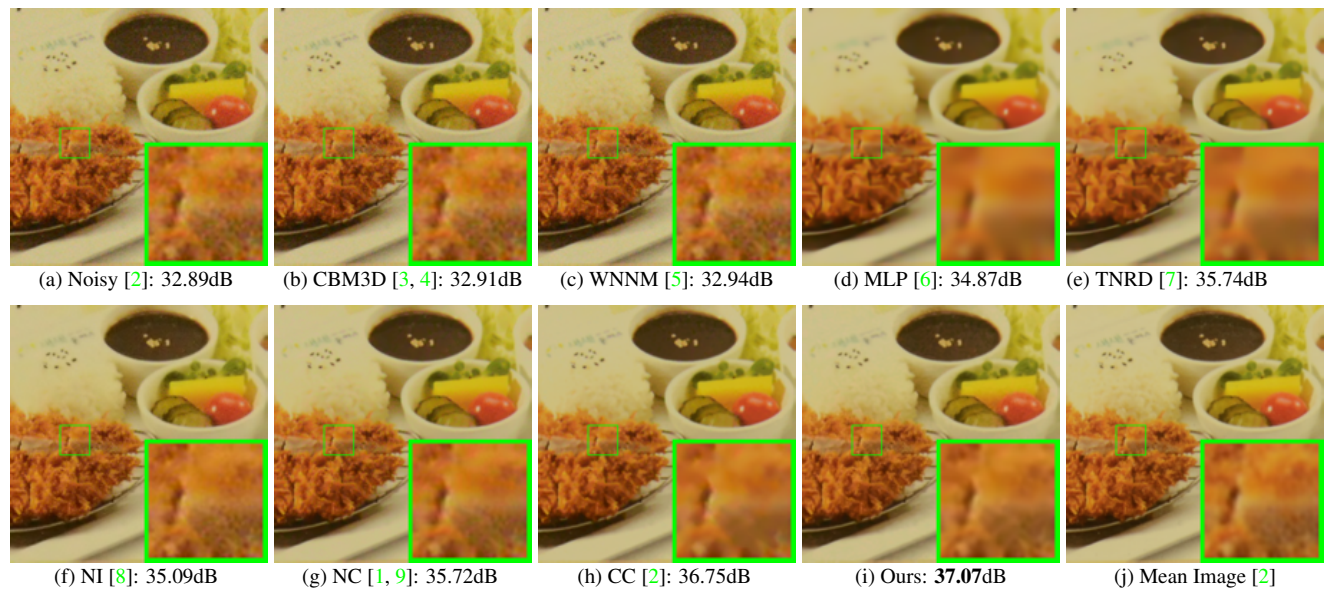


Figure 8. Denoised images of a region cropped from the real noisy image “Nikon D800 ISO 3200 2” [2] by different methods. The images are better to be zoomed in on screen.

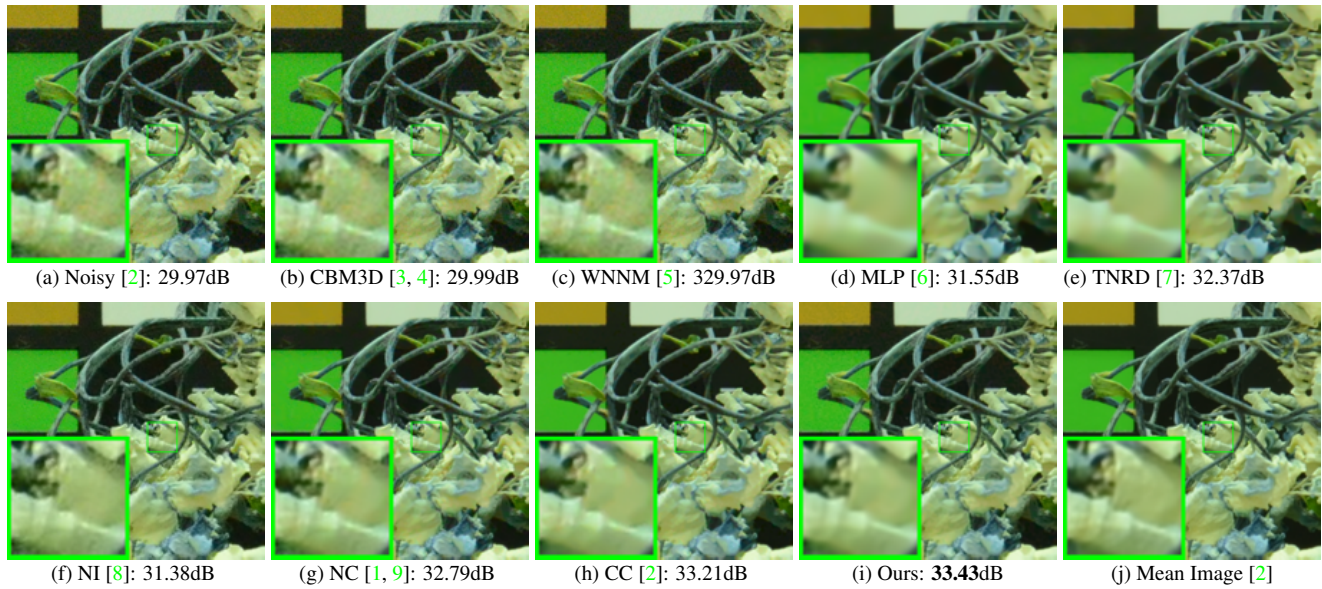


Figure 9. Denoised images of a region cropped from the real noisy image “Nikon D800 ISO 6400 2” [2] by different methods. The images are better to be zoomed in on screen.

#### 4. More Denoising Results on the 60 Cropped Real Noisy Images from [2]

In this section, we provide more visual comparisons of the proposed method with the state-of-the-art denoising methods on the 60 cropped real noisy images we cropped from [2]. In this dataset, each scene was shot 500 times under the same camera and camera setting. The mean image of the 500 shots is roughly taken as the “ground truth”, with which the PSNR can be computed. As can be seen from Figures 10-20, in most cases, our proposed method achieves better performance than the competing methods. This validates the effectiveness of our proposed external prior guided internal prior learning framework for real noisy image denoising.

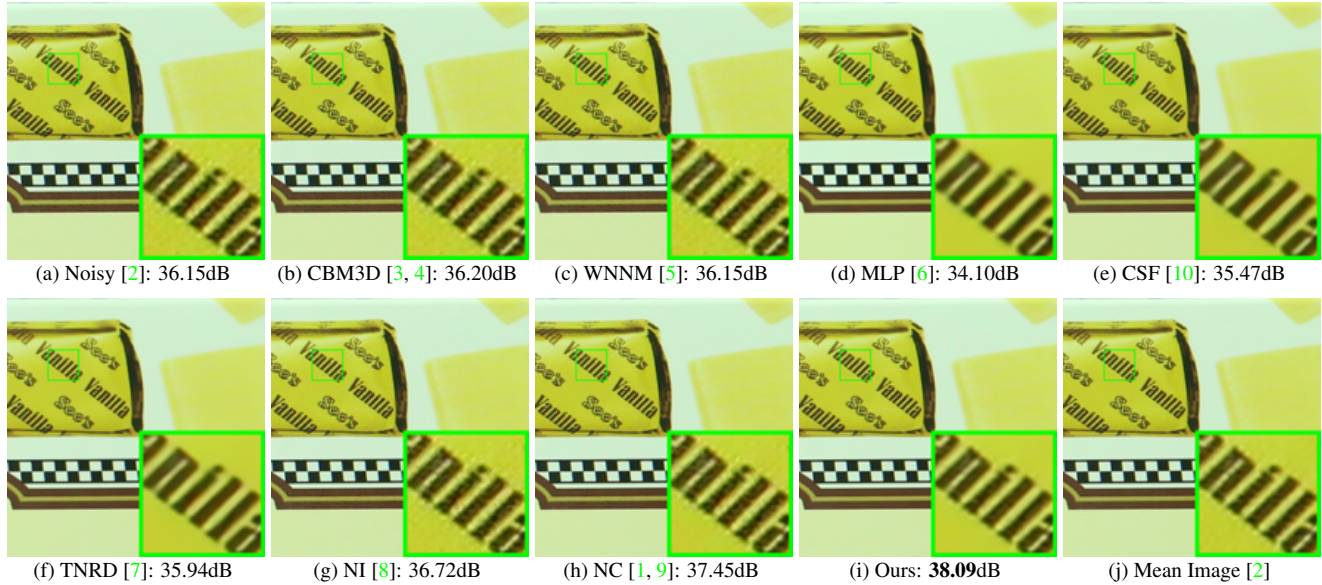


Figure 10. Denoised images of a region cropped from the real noisy image “Canon EOS 5D Mark3 ISO 3200 C1” [2] by different methods. The images are better viewed by zooming in on screen.

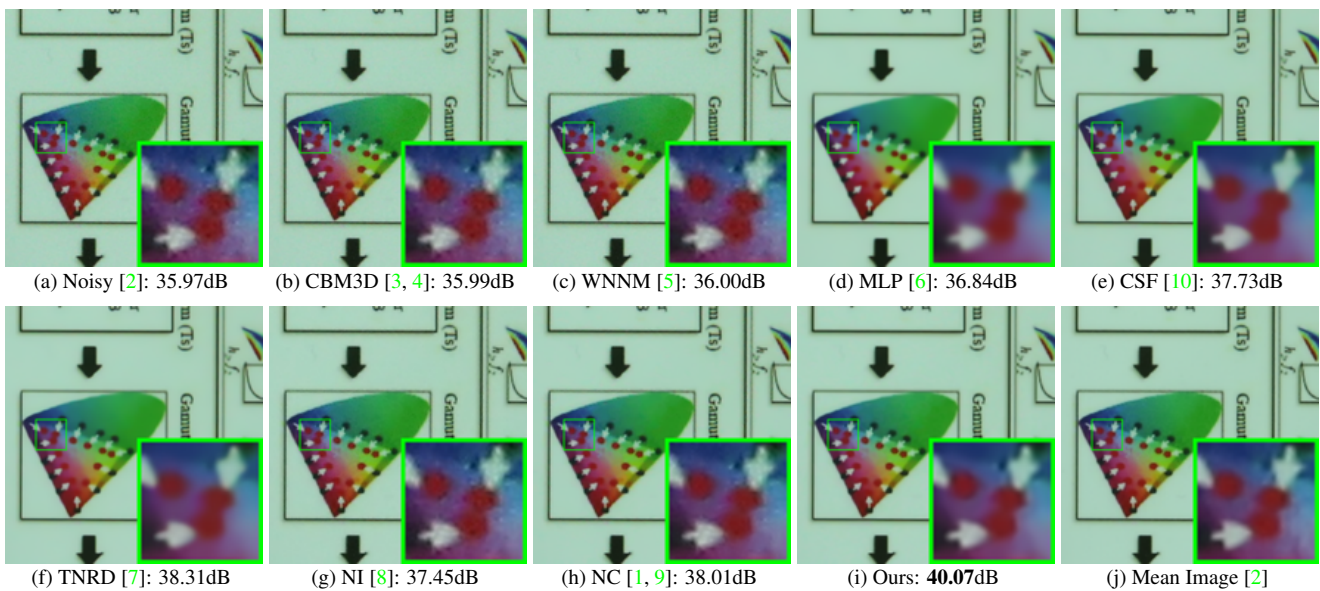


Figure 11. Denoised images of a region cropped from the real noisy image “Canon EOS 5D Mark3 ISO 3200 C2” [2] by different methods. The images are better viewed by zooming in on screen.

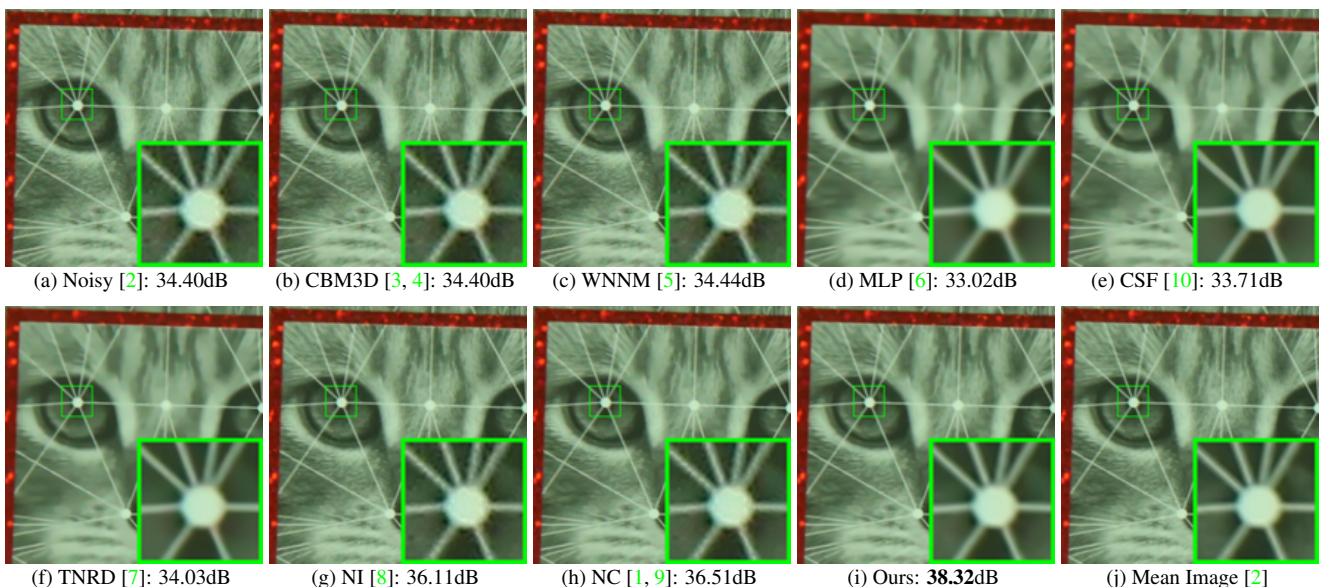


Figure 12. Denoised images of a region cropped from the real noisy image “Canon EOS 5D Mark3 ISO 3200 C3” [2] by different methods. The images are better viewed by zooming in on screen.

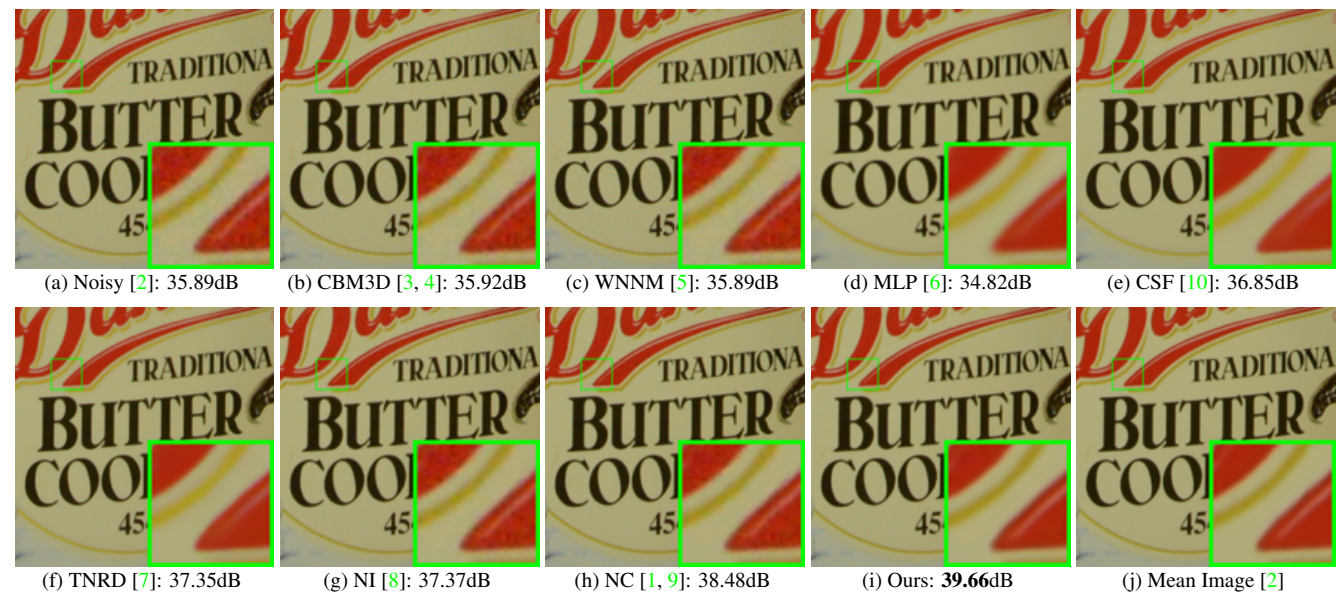


Figure 13. Denoised images of a region cropped from the real noisy image “Nikon D600 ISO 3200 C1” [2] by different methods. The images are better viewed by zooming in on screen.

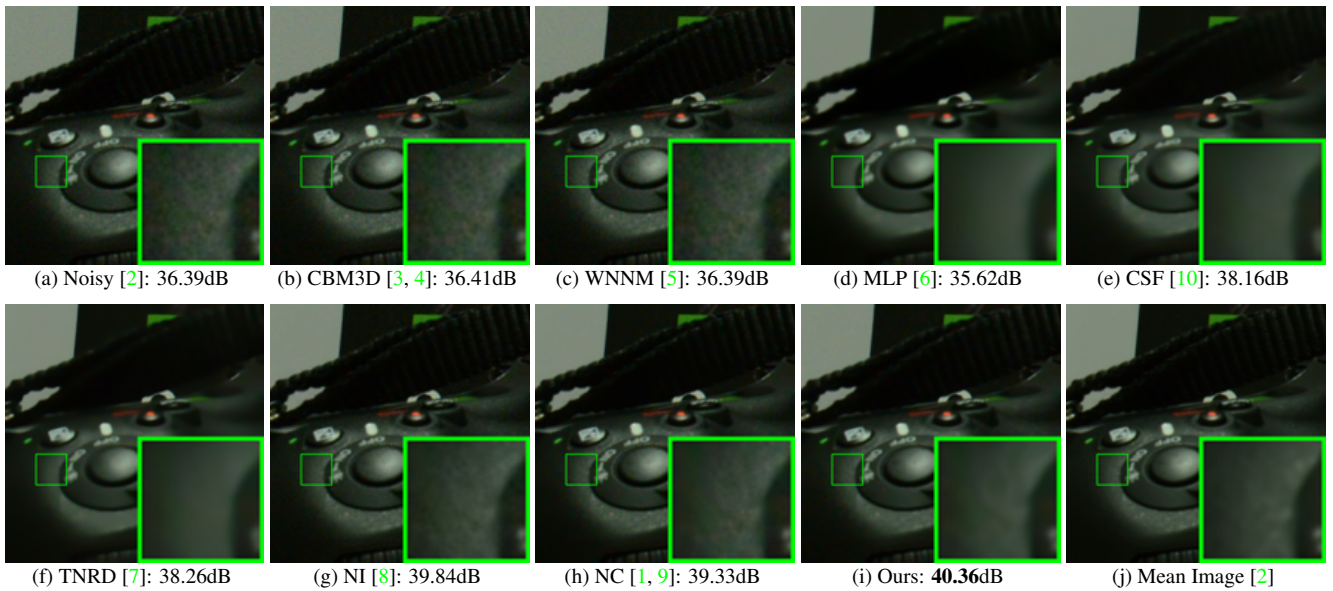


Figure 14. Denoised images of a region cropped from the real noisy image “Nikon D600 ISO 3200 C2” [2] by different methods. The images are better viewed by zooming in on screen.



Figure 15. Denoised images of a region cropped from the real noisy image “Nikon D800 ISO 1600 B2” [2] by different methods. The images are better viewed by zooming in on screen.

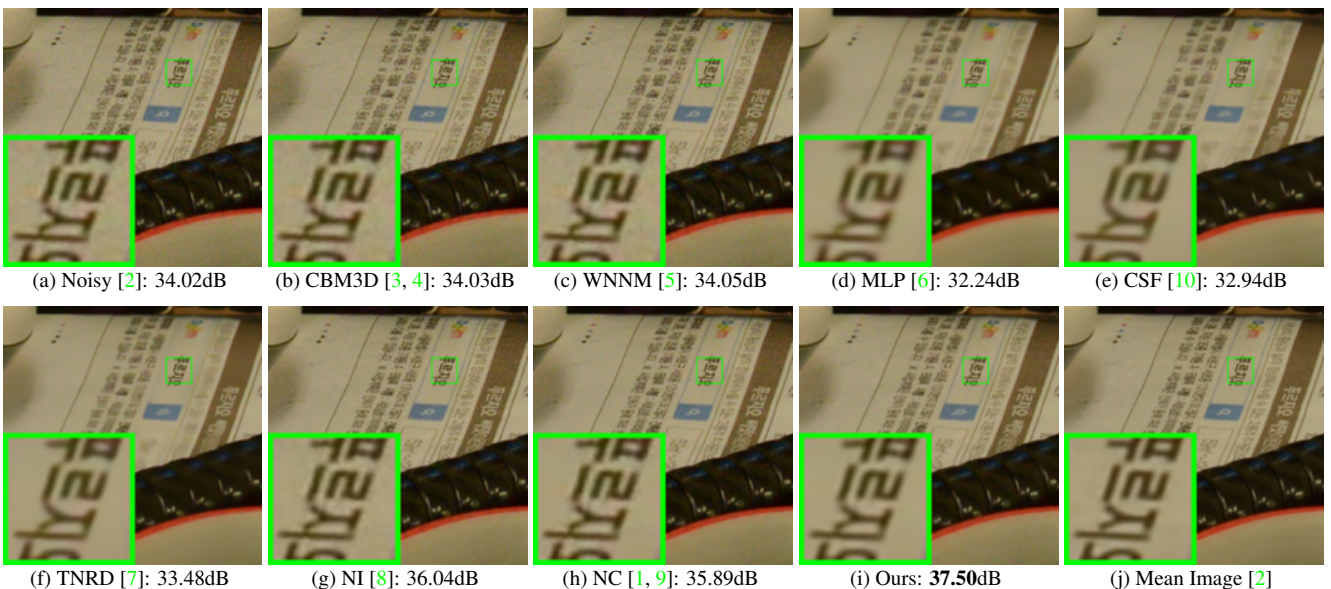


Figure 16. Denoised images of a region cropped from the real noisy image “Nikon D800 ISO 3200 A1” [2] by different methods. The images are better viewed by zooming in on screen.

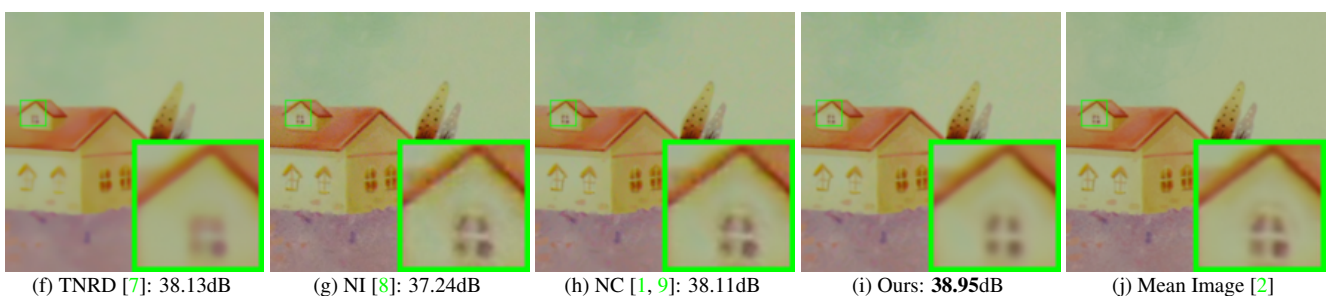
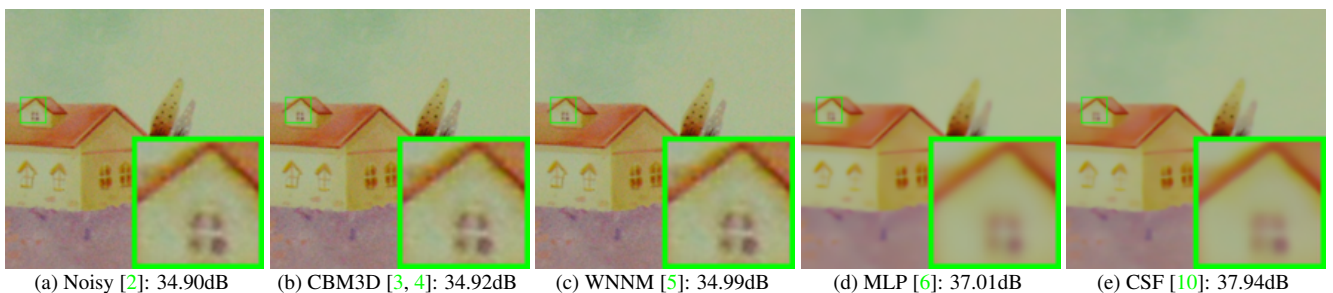


Figure 17. Denoised images of a region cropped from the real noisy image “Nikon D800 ISO 3200 A2” [2] by different methods. The images are better viewed by zooming in on screen.

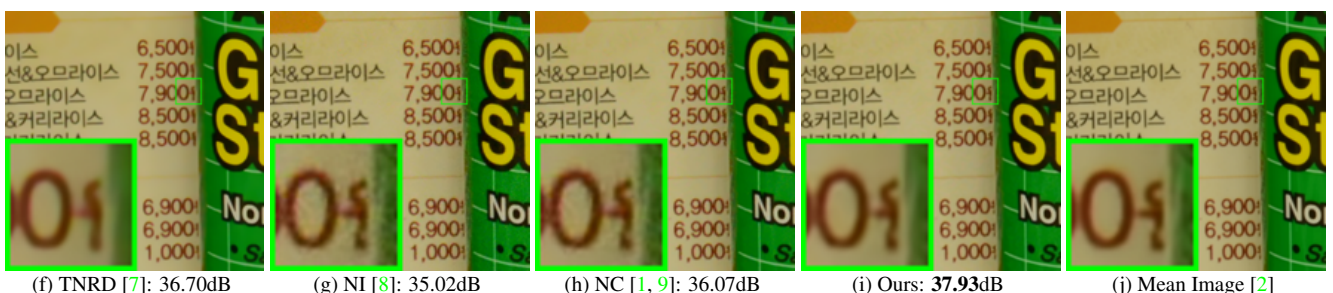
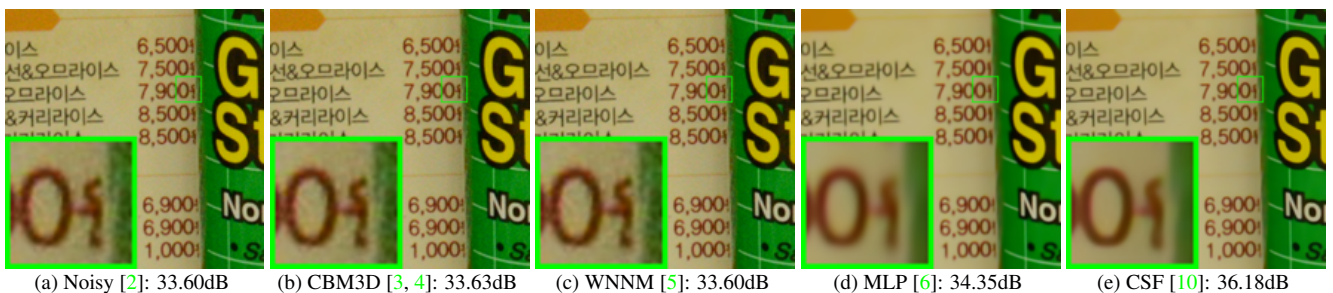


Figure 18. Denoised images of a region cropped from the real noisy image “Nikon D800 ISO 3200 A3” [2] by different methods. The images are better viewed by zooming in on screen.

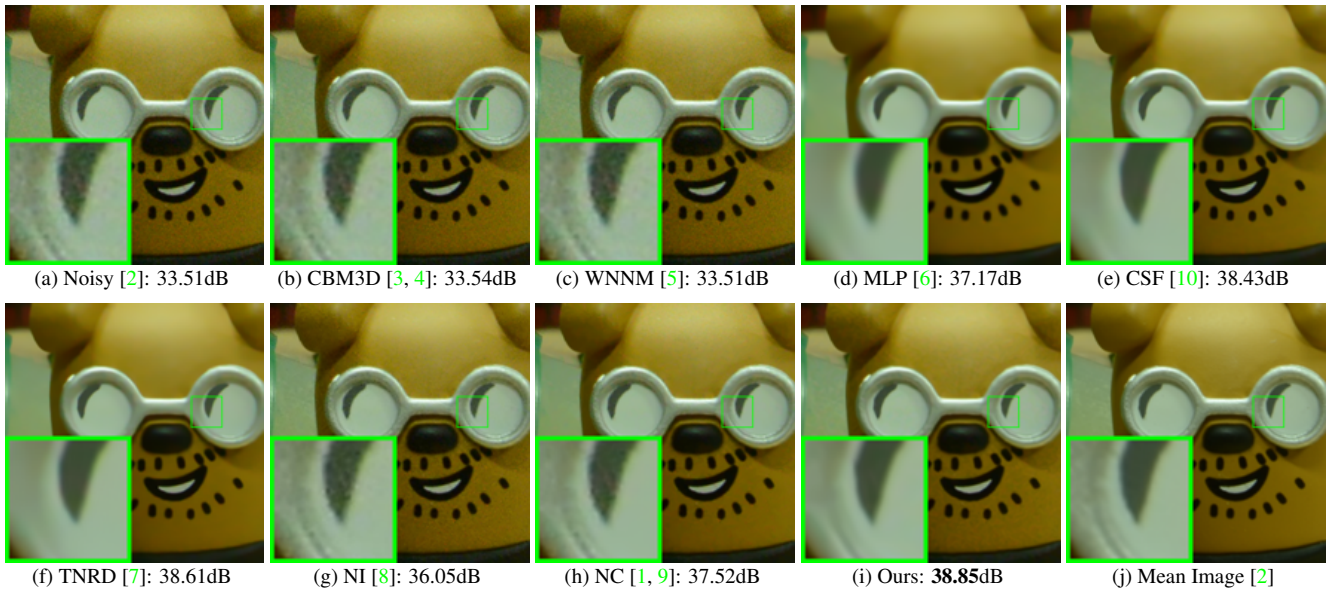


Figure 19. Denoised images of a region cropped from the real noisy image “Nikon D800 ISO 3200 A4” [2] by different methods. The images are better viewed by zooming in on screen.

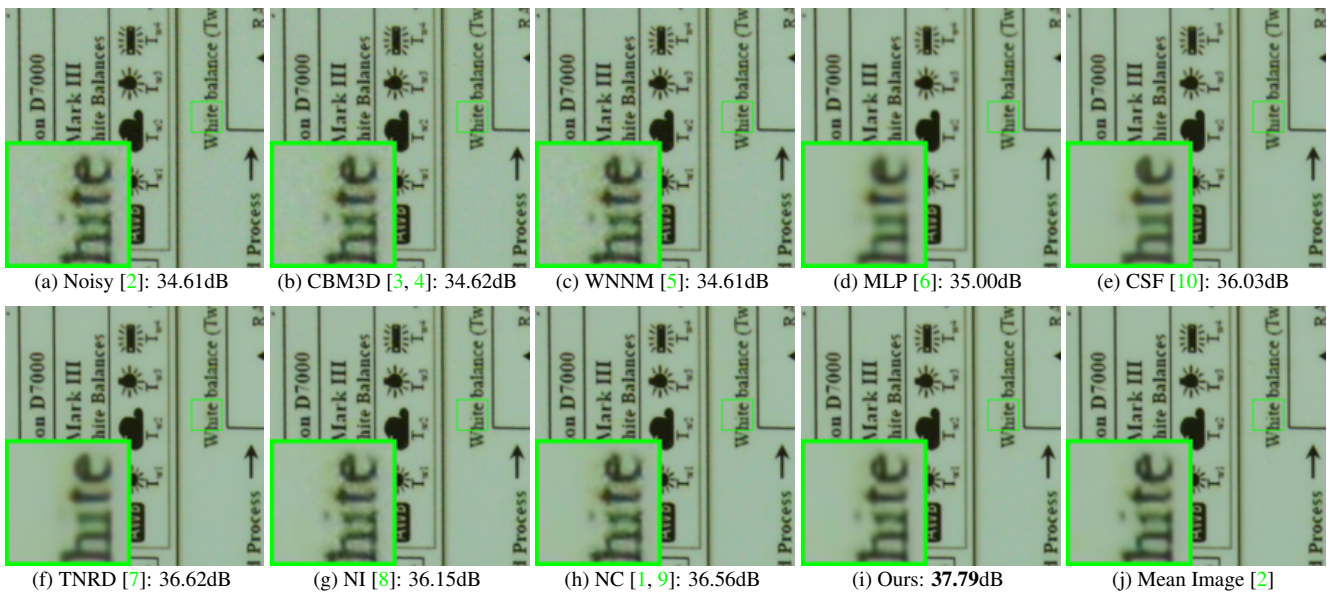


Figure 20. Denoised images of a region cropped from the real noisy image “Nikon D800 ISO 3200 A5” [2] by different methods. The images are better viewed by zooming in on screen.

## References

- [1] M. Lebrun, M. Colom, and J. M. Morel. The noise clinic: a blind image denoising algorithm. <http://www.ipol.im/pub/art/2015/125/>. Accessed 01 28, 2015. 1, 2, 3, 4, 5, 6, 7, 8, 9, 10, 11
- [2] S. Nam, Y. Hwang, Y. Matsushita, and S. J. Kim. A holistic approach to cross-channel image noise modeling and its application to image denoising. *IEEE Conference on Computer Vision and Pattern Recognition (CVPR)*, pages 1683–1691, 2016. 1, 3, 4, 5, 6, 7, 8, 9, 10, 11
- [3] K. Dabov, A. Foi, V. Katkovnik, and K. Egiazarian. Image denoising by sparse 3-D transform-domain collaborative filtering. *IEEE Transactions on Image Processing*, 16(8):2080–2095, 2007. 2, 3, 4, 5, 6, 7, 8, 9, 10, 11

- 1188 [4] K. Dabov, A. Foi, V. Katkovnik, and K. Egiazarian. Color image denoising via sparse 3D collaborative filtering with grouping  
1189 constraint in luminance-chrominance space. *IEEE International Conference on Image Processing (ICIP)*, pages 313–316, 2007. 2, 1242  
1190 3, 4, 5, 6, 7, 8, 9, 10, 11 1243  
1191 [5] S. Gu, L. Zhang, W. Zuo, and X. Feng. Weighted nuclear norm minimization with application to image denoising. *IEEE Conference*  
1192 *on Computer Vision and Pattern Recognition (CVPR)*, pages 2862–2869, 2014. 2, 3, 4, 5, 6, 7, 8, 9, 10, 11 1244  
1193 [6] H. C. Burger, C. J. Schuler, and S. Harmeling. Image denoising: Can plain neural networks compete with BM3D? *IEEE Conference*  
1194 *on Computer Vision and Pattern Recognition (CVPR)*, pages 2392–2399, 2012. 2, 3, 4, 5, 6, 7, 8, 9, 10, 11 1245  
1195 [7] Y. Chen, W. Yu, and T. Pock. On learning optimized reaction diffusion processes for effective image restoration. *IEEE Conference*  
1196 *on Computer Vision and Pattern Recognition (CVPR)*, pages 5261–5269, 2015. 2, 3, 4, 5, 6, 7, 8, 9, 10, 11 1246  
1197 [8] Neatlab ABSoft. Neat Image. <https://ni.neatvideo.com/home>. 2, 3, 4, 5, 6, 7, 8, 9, 10, 11 1247  
1198 [9] M. Lebrun, M. Colom, and J.-M. Morel. Multiscale image blind denoising. *IEEE Transactions on Image Processing*, 24(10):3149–  
1200 3161, 2015. 2, 3, 4, 5, 6, 7, 8, 9, 10, 11 1248  
1201 [10] U. Schmidt and S. Roth. Shrinkage fields for effective image restoration. *IEEE Conference on Computer Vision and Pattern Recog-*  
1202 *nition (CVPR)*, pages 2774–2781, June 2014. 6, 7, 8, 9, 10, 11 1249  
1203  
1204  
1205  
1206  
1207  
1208  
1209  
1210  
1211  
1212  
1213  
1214  
1215  
1216  
1217  
1218  
1219  
1220  
1221  
1222  
1223  
1224  
1225  
1226  
1227  
1228  
1229  
1230  
1231  
1232  
1233  
1234  
1235  
1236  
1237  
1238  
1239  
1240  
1241